Optimization of single-qubit gate fidelities in silicon quantum computers in the presence of crosstalk

Nicky Wanningen (5102952)

Bachelor End Project
BSc Applied Mathematics &
BSc Applied Physics
Delft University of Technology

Delft, August 16, 2022
Supervisors:
Prof. Dr. Ir. L.M.K. Vandersypen,
Dr. M. Möller
Daily supervisor: B.W. Undseth MSc

Abstract

For scaling up the qubits in silicon quantum computers, it is vital to determine crosstalk effects that can lower the fidelity of the computer. In this computational project, we examine single-qubit gate-fidelities in the presence of crosstalk for uncoupled spin qubits that are driven with X-gates via electron dipole spin resonance (EDSR). We introduce two models: the first model introduces the AC Stark shift and the novel second model expands on this by adding a resonance frequency shift on top. We assume the latter resonance frequency shift to be due to heating effects. We optimize the gate-fidelity for a qubit coupled to up to six drives as a function of the overall driving time and -frequency of a single drive for both models using the Nelder-Mead algorithm.

Using the AC Stark shift model, we still obtain 0.99999 fidelity if we do not account for the crosstalk. However, when using the second model, the fidelity drops to 0.69 in the presence of two drives when we do not correct for the heating-induced resonance frequency shift and the AC Stark shift. Furthermore, the fidelity decreases linearly with the number of drives coupled to the qubit, implicating that the resonance frequency shift will become a significant problem for the scalability of silicon quantum computers. We find that we can correct for the resonance frequency shift entirely by using optimized driving time and -frequency, where most gain comes from optimizing the driving frequency. Moreover, we discover that there is a linearly increasing dependence of the resonance frequency shift at the theoretical driving time as a function of the total drives. Up to a translation factor of 0.5 MHz, we discover the same linear relationship for the correction needed on the theoretical driving frequency to hit maximum fidelity as a function of the total drives.

Table of Contents

1

Introduction

A lot of effort has been directed into designing quantum systems that can function as computers, so-called quantum computers. The advantage of quantum computers over classical computers is that quantum computers can perform specific tasks orders of magnitude faster than classically possible. Spin qubits are quantum bits that form a two-level system based on the spin of an electron or the absence of an electron, called an electron-hole, in semiconductor devices. Due to the nature of spin-qubits, we can control how they behave via magnetic and/or electric fields. Using spin qubits for quantum computing was first proposed back in 1998 [10], and silicon-based quantum computing is a promising platform for quantum computers due to their small size and relatively long memory lifetime (called coherence time). In addition, semiconductor quantum devices could be easily integrated into the existing semiconductor manufacturing infrastructure [23],[28]. During the past 20 years, a lot of advances in the area have been made and, recently, it has been demonstrated that universal control of six qubits in a silicon quantum computer is possible [16], which would correspond to 64 bits on a classical computer.

To enable reliable large-scale quantum computing, it is necessary to scale up the number of qubits while maintaining high fidelities, which is a measure of how trustworthy the computer performs its operations on the qubits. One of the errors that can lower the fidelity of a quantum processor is crosstalk, which are errors due to some subsystem of the computer unintentionally influencing another subsystem [21],[26]. To correct for crosstalk, it is essential to investigate its origin and consequences. The aim of this thesis is to evaluate and optimize the fidelity of a single qubit in a two- to six-qubit system that feels two types of crosstalk due to the operations that are performed on the other qubits.

Before we can calculate the fidelity, we first build a model in which spin-qubits are driven via a method called electron dipole spin resonance (EDSR). This method uses a combination of magnetic fields in such a way that we can perform operations on the qubits individually by using magnetic fields that oscillate at a qubit-specific frequency, called the qubit's resonance frequency. This frequency is different for all the qubits in the system, enabling us to perform various operations on other qubits. Next, we introduce the AC Stark shift in the model, which is a type of crosstalk that shifts the resonance frequency of the qubits as a consequence of the qubits 'feeling' not only the operation we intend it to feel, but also the operations on other qubits, driven with different frequencies. Furthermore, "AC" stands for the alternating source of the drives. To expand on this model, we introduce a resonance frequency shift of unknown nature that has been observed by several research groups [3],[24],[20],[29],[16]. We assume that this form of crosstalk is due to the energy that the magnetic fields performing the qubit operations feed into the system, which heats the qubits. We calculate the fidelities of a qubit that is influenced by the crosstalk in both models (AC Stark shift with and without heating). Afterward, in the hope of correcting for the crosstalk effects, we use an optimization algorithm, the Nelder-Mead simplex algorithm, to find the optimal operation time and the optimal frequency for performing an operation on the qubit to get the optimal fidelity for said qubit.

This thesis is structured as follows. The theoretical background, including the Nelder-Mead algorithm needed for this project, is contained in chapter 2. We explain the model in chapter 3 and the results are presented in chapter 4. We discuss the limitations of the model and the implications of the results in chapter 5. The conclusion of this thesis can be found in chapter 6.

2

Theory

The purpose of this chapter is to give the theoretical background that forms the basis of this thesis. We cover the basic mathematics behind quantum gates on qubits, a way to perform quantum operations in the laboratory called EDSR and a characterization of how well these operations are performed as compared to the ideal operations. Lastly, we present an optimization algorithm called Nelder-Mead which we will use to maximize the performance of our qubit operations for a given set of parameters.

2.1. Qubits and qubit operations

The memory cells of our quantum computer are qubits and we can represent their value, the so-called qubit state, as a superposition of the set of statevectors forming an orthonormal basis in the 2-dimensional Hilbert space $\mathcal{H}_2$. We can choose any orthonormal basis, but for simplicity we pick the following basis:

$$\left\{ \quad |0\rangle = \begin{pmatrix} 1 \\ 0 \end{pmatrix} \quad , \quad |1\rangle = \begin{pmatrix} 0 \\ 1 \end{pmatrix} \quad \right\},$$

which basisvectors $|0\rangle$ and $|1\rangle$ are called 'up' and 'down', respectively. Our qubit state $|\psi\rangle \in \mathcal{H}_2$ is then given by:

$$|\psi\rangle = \alpha |0\rangle + \beta |1\rangle \quad , |\alpha|^2 + |\beta|^2 = 1 \quad , \quad \alpha, \beta \in \mathbb{C} \quad .$$

An alternative to the representation above is $|\psi\rangle = \cos\frac{\theta}{2}|0\rangle + e^{i\phi}\sin\frac{\theta}{2}|1\rangle$ with $\theta \in [0,\pi]$ and $\phi \in [0,2\pi)$. All possible states can then be easily visualized with the help of the Bloch sphere, see figure 2.1.
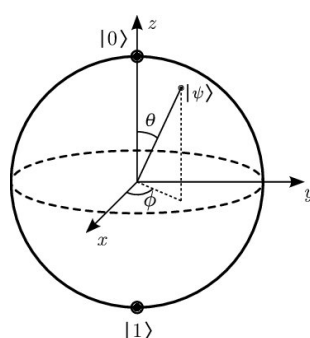
Figure 2.1: A statevector of a qubit represented on the Bloch sphere. The sphere has a radius of 1 and the vectors of the orthonormal basis are on both sides of the z-axis. Pure qubit states can be represented by the coordinates (θ, ϕ) on the Bloch sphere. Mixed qubit states are represented by the coordinates (r, θ, ϕ) for some $r \in \mathbb{R}$ with r < 1, which correspond to points within the Bloch sphere. The figure was taken from [19] and is unchanged (available via license: CC BY 4.0).

In order to make use of qubits, we need to be able to perform operations on them, which we call quantum gates. Gates change the state of the qubit, which we can visualize as changing from one point on/in the Bloch sphere to another point on/in the sphere. An important characterization of quantum gates is that they are unitary, which makes the gates norm preserving.

Possible (single-qubit) gates are the X-, Y- and Z-gates, which rotate the qubit's state by 180 degrees around the x-, y- or z-axis, respectively:

$$X = \hat{\sigma}_x \quad , \quad Y = \hat{\sigma}_y \quad , \quad Z = \hat{\sigma}_z \quad ,$$

with $\hat{\sigma}_x, \hat{\sigma}_y, \hat{\sigma}_z$ the Pauli matrices. Note that performing an X- or Y-gate on a qubit in up- or down-state is indistinguishable from one another except for a phase constant. Another possible gate is the SWAP-gate, which is a two-qubit gate that swaps the states of two qubits. Another two-qubit gate is the CNOT gate, which flips the value of a qubit if and only another qubit is in an up-state. In systems with more than one qubit, single and multiple qubit gates can be combined using tensor products, which are notated with the ⊗ symbol. For instance, performing an X-gate on qubit 1 and a Y-gate on qubit 2 would result in a total quantum gate of $X \otimes Y$.

2.2. Time evolution

To get the full picture of how qubits work, we also need to know how qubits behave in time. For this, we turn to the qubit's Hamiltonian $\hat{H}$, which tells us the kinetic and potential energy of our qubit. The Schrödinger equation $i\hbar \frac{\partial \psi}{\partial t} = \hat{H}\psi$ then tells us the time evolution of the qubit, where $\hbar$ is Planck's constant divided by 2π [14].

Instead of constantly solving this differential equation, we can also find a direct formula for the time evolution using the propagator $\hat{U}(t)$, given an initial state $|\psi(0)\rangle$:

$$|\psi(t)\rangle = \hat{U}(t)|\psi(0)\rangle \quad .$$

The propagator can be calculated from the Hamiltonian $\hat{H}$. For a time-dependent Hamiltonian, the propagator can be computed as follows:

$$\hat{U}(t) = \mathcal{T}\left[\exp\left(\frac{-i}{\hbar}\int_0^t \hat{H}(\tau)d\tau\right)\right] \quad , \tag{2.1}$$

where $\mathcal{T}$ is the time-ordering operator. This calculation is not has no closed-form solution and to solve this one would need to turn to a numerical simulation. However, for a time-independent Hamiltonian equation 2.1 simplifies [8]:

$$\hat{U}(t) = \exp\left(\frac{-i\hat{H}t}{\hbar}\right) \quad . \tag{2.2}$$

2.3. Electron dipole spin resonance

To be able to make use of the qubits, we need a way to perform the quantum gates on them. One method of doing this is called electron dipole spin resonance (EDSR). [17] This technique cleverly makes use of a slanted static external magnetic field $\vec{B}_z$, which ensures we can address the qubits separately from one another, and an effective alternating magnetic field $\vec{B}(t)$ to perform the quantum gates, also further referred to as 'the drive'.

2.3.1. Effective Hamiltonian

The potential energy of a qubit in the presence of a magnetic field is given by the Hamiltonian $H = -\vec{\mu} \cdot \vec{B}$, where $\vec{\mu} = \frac{-g\mu_B \vec{S}}{\hbar}$, in which g is the Landé g-factor, μ_B is the Bohr magneton, $\hbar$ is Planck's constant divided by 2π and $\vec{S}$ is the spin operator. By now applying a static magnetic field in the z-direction, the energy levels of the qubit get separated, which is known as 'Zeeman splitting'. The contribution of the static magnetic field to the Hamiltonian is $H_s = -\frac{\omega}{2}Z$, where Z is the Z-gate and $\omega = \frac{g\mu_B B}{\hbar}$ (with B the static magnetic field strength) is called the Larmor frequency [4]. The contribution of the alternating magnetic field $\vec{B}(t) = \Omega\cos(\tilde{w}t)$ in the x-direction is $H_{ac}(t) = \Omega\cos(\tilde{w}t)X$, where Ω is the drive strength of the magnetic field and $\tilde{w}$ is the driving frequency. For qubits that undergo no qubit-qubit interactions, our effective total single-qubit Hamiltonian when driving an X-gate looks as follows:

$$H(t) = -\frac{\omega}{2}Z + \frac{\Omega}{2}\cos(\tilde{w}t)X \quad . \tag{2.3}$$

2.3.2. Driving time

We clearly see the EDSR Hamiltonian and our drive are time-dependent. As a consequence, if we want to drive a certain gate on a qubit, it matters for how long we keep driving the qubit with the alternating magnetic field. For instance, if we would like to perform a perfect X-gate, having a driving time that is too short or long, results in a rotation around the x-axis that is not a perfect 180 degrees. The driving time τ for an X- and Y-gate depends on the driving strength Ω by $\tau = \frac{2\pi}{\Omega}$.

2.3.3. Rotating wave approximation

So far, everything that has been considered has been done in the laboratory frame of the qubit. In some cases, converting the qubit to the rotating frame of the qubit can simplify calculations or offer valuable insight into the dynamics. Transforming the Hamiltonian to the rotating frame of the qubit, notated by $\tilde{H}$, can be achieved with $\tilde{H} = RH(t)R^\dagger + i\frac{dR}{dt}R^\dagger$, where $R = \exp(\frac{-i\omega t Z}{2})$, with all the other parameters defined as above. Transforming the propagator U to the rotating frame is achieved with the formula $\tilde{U} = RU$. When we mention an ideal operation being some gate, we mean that this gate defined in the rotating frame of that qubit. This is because said rotating frame removes the effect of the precession around the z-axis that is due to the external magnetic field on the qubit, which is a movement the qubit does regardless of which operation we perform on the qubit.

For drives that have a small detuning from the resonance frequency of the qubit, we can make an approximation for the Hamiltonian in the rotating frame [27]. Since the fast rotating terms of the Hamiltonian evaluate to zero when integrating over relatively large times, we can ignoring these fast rotating terms. We call this the Rotating Wave Approximation (RWA). Conveniently enough, the time-dependent Hamiltonian in equation 2.3 evaluates to the following time-independent Hamiltonian in the rotating frame

$$\tilde{H}_{RWA} = -\frac{\omega - \tilde{w}}{2}Z + \frac{\Omega}{4}X \quad .$$

To extract the propagator from the Hamiltonian above, we can then use equation 2.2. Physically, the effect of driving the qubit with a slightly off-resonant frequency causes the qubit to undergo perturbed Rabi-oscillations with a frequency of $\sqrt{(\Omega/2)^2 + (\Delta w)^2}$, where Δw is the detuning of the drive. Rabi-oscillations describe the periodic flopping of a qubit from one of its eigenstates (up- and down-state) to the other in the presence of a slightly detuned drive [4].

However, when an qubit gets driven with multiple drives with different driving frequencies, we cannot use the RWA anymore since the detuning of all the different drives together is not small enough anymore for the RWA to be applicable [5]. Thus, the Hamiltonian remains time-dependent, which makes extracting the propagator hard. Another way of approximating the propagator directly is by using the Floquet-Magnus Expansion [11]. However, in this project we turn to the numerical ODE solvers of Python 3's QuTiP package to calculate the propagators, since we can control numerical errors more easily than errors in approximating the propagator itself. Numerical methods aim to approximate the solution (which is a function) of a differential equation by discretization of the grid function at points in the domain of the function we solve for. After discretization, numerical algorithms give a recipe for how to go about approximating the solution of the function at the different points of the domain. To calculate the propagators, the numerical methods solve another form of the time-dependent Schrödinger equation: $i\hbar\frac{\partial U(t,t_0)}{\partial t} = \hat{H}U(t, t_0)$ with the initial value $U(t_0, t_0) = I$, where I is the identity operation in $\mathcal{H}_2$ in the case we consider a 2-dimensional Hamiltonian. For a detailed explanation of the methods that are used for solving said equation, we refer to the sections on Adam-Moulton methods and Backwards Differentiation Formulas in paper [2].

2.4. Fidelity

Next, we would like to know if the operations that we perform on the qubits are the same as we intend them to be. We characterize this by calculating the gate fidelity of one or more qubits within the system. The gate fidelity compares the actual performed operation with the intended operation and averages over all possible initial states that the qubits could have. The gate fidelity can be found in the following equation:

$$F(t) = \frac{d + |\text{Tr}[U^\dagger_{ideal}(t)U_{actual}(t)]|^2}{d(d+1)} \quad , \tag{2.4}$$

in which d is the dimension of the Hamiltonian of the qubits we are interested in, U_{actual} is the propagator of the performed qubit operation and U_{ideal} is the propagator of the intended qubit operation. This formula rests on the diagonalizability of Hermitian matrices and on the fact that any matrix can be split into a Hermitian

and an anti-Hermitian counterpart [15]. To find the fidelity of a certain gate, we can take the time t in the above equation to be equal to the driving time.

For a quantum computer to become scalable, we need to achieve very high fidelities. For instance, 0.99 fidelity corresponds to 1 in a 100 operations generating an error. Thus, for quantum computers to become reliable enough to work with, we need a fidelity that has a value that is extremely close to 1.

2.5. Crosstalk

One phenomenon that affects the gate fidelities in an experimental set-up is called crosstalk. Crosstalk is any kind of unintended influence that some subsystem of our set-up exercises on another subsystem. Within experimental quantum computing, there exist several kinds of crosstalk, such as AC stark shift, heating effects and coupling of the qubits [26]. For the purpose of this thesis, we only elaborate on the AC stark shift and we introduce an additional resonance frequency shift that has not been understood yet.

2.5.1. AC stark shift

The AC Stark shift is a crosstalk effect caused by capacitively induced gate coupling of the driving fields of EDSR that are meant to drive gates on other nearby qubits. In essence, the qubit of interest is then driven by several off-resonant drives, resulting in an off-resonant Rabi-oscillation with a detuned Rabi frequency. Effectively, this means that the qubit's axis of quantization, the axis on which the up- and down-state are defined, changes slightly. Because of this, the qubits resonance frequency changes slightly together with the new quantization axis.

More specifically, the AC Stark shift is caused by an alternating (hence the 'AC') and non-resonant field of the form $V_{or} \cos(w_{or} t)/2$, where w_{or} is the off-resonance frequency of the drive and V_{or} the driving strength of the off-resonant drive. We can move into the rotating frame of the difference between the on-resonant and off-resonant drive with frequency $\Delta w_{or} = w_0 - w_{or}$, where w_0 is the on-resonance frequency. Next, we apply the RWA to arrive at the following Hamiltonian: $H_{RWA} = \Delta w_{or} Z/2 + \Omega_{or} X/2$, where Ω_{or} is the amplitude of the off-resonant Rabi-oscillation. We can now define a new quantization axis with an effective detuning of $\Delta w_{eff} = \sqrt{\Delta w_{or}^2 + \Omega_{or}^2}$. The original frame of reference was rotation at w_0, so the new resonance frequency becomes $w_{res} = w_0 + \Delta w_{eff}$, which approximates to $w_{res} \approx w_0 + \frac{\Omega_{or}^2}{2(w_0 - w_{or})}$. The effective resonance frequency shift is given by

$$w_{shift,ACStark} \approx \frac{\Omega_{or}^2}{2(w_0 - w_{or})} \quad , \tag{2.5}$$

where $\Omega_{or} = V_{or}/2$.

2.5.2. Resonance frequency shift

Another phenomenon that has been observed in experimental quantum computing in silicon is a resonance frequency shift of a qubit in the presence of drives on other qubits that has a much larger order of magnitude than the AC Stark shift. Different research groups have observed this shift, but the nature of the shift is unknown [3],[24],[20],[29],[16]. The shift is reportedly about 2 MHz and it is suggested that the frequency change might be due to some property of the quantum dots used in the experimental set-up [24]. In this project, we will model it as if the nature of this shift is heating. The reason for this is that an explicit temperature dependence of the Larmor frequencies has been confirmed in the lab [22]. The precise model for this heating is given in chapter 3.

2.6. Optimization

When trying to correct for crosstalk, we can optimize the gate fidelity of a qubit. In general, in optimization we try to find the best solution out of all feasible solutions for a given set of variables. For optimization for a function $f : \mathbb{R}^n \to \mathbb{R}$ depending on continuous variables, the standard optimization problem looks as follows:

$$\min_x \quad f(x)$$
$$\text{s.t.} \quad a_i(x) \le 0, i = 1,...,l$$
$$\qquad b_j(x) = 0, j = 1,...,k$$

where $f(x)$ is called the objective function that depends on a vector $x \in \mathbb{R}^n$, which represents the n-variables that we optimize for. The functions $a_i, b_j : \mathbb{R}^n \to \mathbb{R}$ for $l, p \geq 0$ represent the inequality and equality constraints, respectively, that we put on the objective function. We can write a maximization problem as a minimization problem by simply minimizing the negative objective function of the maximization problem. Furthermore, we call the optimization problem unconstrained when $l, p = 0$. [7]

2.6.1. Nelder-Mead optimization

The Nelder-Mead algorithm (NM) aims to minimize a scalar-valued objective function for one or more variables. [13] NM is a direct search method, meaning that it does not use any derivative information about the scalar functions. Instead, it relies on evaluating the function values for test-points that lie on a simplex, which is an n-dimensional geometric object that has $n + 1$ vertices. Based on the function values, the algorithm chooses more test-points and adapts the shape of the simplex in the direction of the best function value. It discards the test points with the worst function values by moving away from them. The simplex so to say 'walks' over the landscape of the objective function's range. By the direction of the 'best' value is meant that when we see the function value decrease, it is considered to be in the direction of the minimum we aim to find. As a consequence of this, the Nelder-Mead algorithm can converge to a local minimum instead of a global minimum, depending on which starting test-points are chosen. Checking if the algorithm finds a global minimum can be effectively done with a brute-force grid search over the optimization variables. The grid search will output the fidelity values for a predefined grid and it gives information about the approximate location of the global optimum.

We proceed to describe the steps of the Nelder-Mead algorithm in more detail. Each iteration of NM has a simplex where the vertices x_i for $i = 1, ..., n + 1$ are points in $\mathbb{R}^n$ with the corresponding function value. The outcome of each iteration is either a new vertex that replaces the worst vertex of the previous simplex, or a set of n new vertices that form a 'smaller' simplex together with the best vertex of the previous simplex. We can perform a total of four operations on the simplex, associated with a corresponding scalar parameter: reflection ρ, expansion χ, contraction γ and shrinkage σ. An iteration of the algorithm is visualized in figure 2.2 and contains the following steps [25], [9]:

1. **Ordering**: the vertices are ordered from the best to worst function value and given the labels x_1 to x_{n+1} respectively.

2. **Reflecting**: calculate the reflection point

$$x_r = \bar{x} + \rho(\bar{x} - x_{n+1}) \quad ,$$

where $\bar{x} = \sum_{i=1}^n x_i / n$. If the function value of this new point is better than the function value of the worst vertex, $f(x_1) \leq f(x_r) < f(x_{n+1})$, the worst function value is replaced by the reflection point and the iteration starts from scratch. If this is not the case, go on to step 3.

3. **Expanding**: if $f(x_r) \leq f(x_1)$, we calculate the expansion point

$$x_e = \bar{x} + \chi(x_r - \bar{x}) \quad .$$

If $f(x_e) < f(x_r)$, we accept x_e as a new vertex and discard x_{n+1} and the iteration starts from scratch. If this is not the case, we will continue with the next step.

4. **Contracting**: if $f(x_r) \geq f(x_n)$ and

   - **Inside contraction**: the value of x_r is strictly better than the value of x_{n+1}, we calculate $x_c = \bar{x} + \gamma(x_r - \bar{x})$. If $f(x_c) \leq f(x_r)$, we accept x_c and discard x_{n+1}. The iteration terminates. Go to step 5 if this is not the case.
   - **Outward contraction**: the value of x_r is worse than the value of x_{n+1}, we calculate $x_c' = \bar{x} - \gamma(\bar{x} - x_{n+1})$. If $f(x_c') \leq f(x_{n+1})$, we accept x_c' and discard x_{n+1}. The iteration terminates. Go to step 5 if this is not the case.

5. **Schrinking**: we define n new vertices v_i for $i = 2, ..., n + 1$ from

$$v_i = x_1 + \sigma(x_i - x_1) \quad ,$$

and we start a new iteration with the simplex that has vertices $x_1, v_2, ..., v_{n+1}$.

Since each iteration is done for a given simplex, an initial simplex and a set of criteria for when to terminate the algorithm have to be specified. Often, programmed algorithms generate this simplex when the algorithm is supplied with an initial guess for one of the vertices.
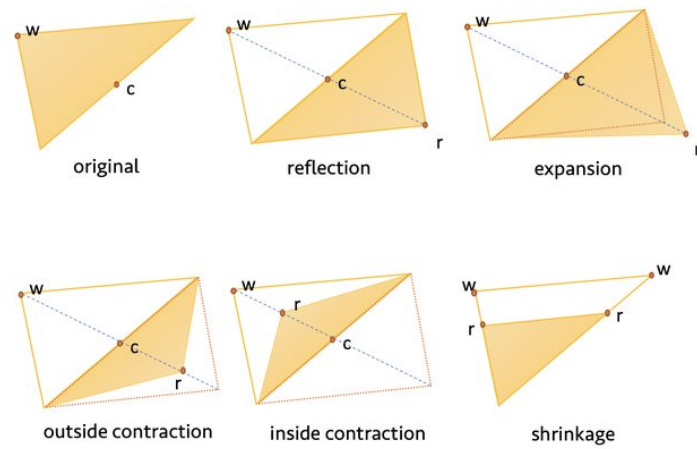
Figure 2.2: Visualization of the different steps of a single iteration in the Nelder-Mead algorithm for a 2-dimensional optimization problem. The original 3-dimensional simplex at the start of the iteration is displayed in the top left corner of the figure. Point 'w' displays the vertex with the worst function value. Point 'c' displays the location of $\bar{x}$. 'r' is the reflection point. The figure was taken from [6] and is unchanged (available via license: CC BY 4.0).

<div style="text-align: right; font-size: 100px; font-weight: bold;">3</div>

Model

In this chapter, we explain the model used in this project. The entire model is programmed in Python3. We present the relevant equations for the Hamiltonian of a single-qubit that is controlled via EDSR and feels the effect of gates being driven on neighbouring qubits. Next, we expand on this model by adding a term that represents the resonance frequency shift as a consequence of heating. We generalize both the model with and without a resonance frequency shift due to heating for a single qubit that is affected by multiple drives, which gives us information about how a single-qubit will behave in a system that encompasses multiple driven qubits in total. Lastly, we present the optimization problem solved by the Nelder-Mead algorithm to find the maximum obtainable single-qubit gate fidelity. The values of all parameters thare are introduced in this chapter can be found in Appendix A.

3.1. AC Stark shift

To examine how the AC Stark shift affects the single-qubit gate fidelity, we take the effective EDSR Hamiltonian from equation 2.3 and expand this model by adding a driving term to this Hamiltonian. We further refer to the effective EDSR Hamiltonian as the 'EDSR Hamiltonian'. The extra driving term represents the influence of a nearby qubit on which a quantum gate is performed for a certain amount of time. Effectively, the qubit in question then feels an extra off-resonant drive. Since X- and Y-gates only differ by a 90 degrees phase factor, we can choose to drive all qubits with a X-or Y-gate without loss of generality. Hence, all drives in this project are X-gates and we set $\hbar = 1$. Moreover, all drives throughout this project have a rectangular pulse envelope. The single-qubit Hamiltonian $H_2 \in \mathcal{H}_2$ of qubit 2 in the presence of qubit 1 is then given by:

$$H_2 = -\frac{w_2}{2}\hat{\sigma}_z + \frac{\Omega_2}{2}\cos(w_2 t)\hat{\sigma}_x + \alpha\frac{\Omega_1}{2}\cos(w_1 t)\hat{\sigma}_x \quad, \tag{3.1}$$

where w_1 and w_2 are the resonance frequencies in units of rad Hz of the qubit 1 and qubit 2, respectively, Ω_1 and Ω_2 are the driving amplitudes in units of rad Hz of the X-gates being performed on qubit 1 and qubit 2, respectively, and α is the unitless crosstalk factor that represent how much the drive of qubit 1 couples to qubit 2.

Ultimately, we would like to know the gate fidelity of qubit 2 by using equation 2.4. We assume all the qubits that we consider are uncoupled and because of this assumption, we can consider single-qubit Hamiltonians instead of considering the Hamiltonian of the whole system. To compute the gate fidelity, we take the actual Hamiltonian H_{actual} to be H_2 in which crosstalk effects are present and we take the ideal Hamiltonian H_{ideal} to be the same as the EDSR Hamiltonian in equation 2.3. The propagators of these (time-dependent) Hamiltonians, U_{actual} and U_{ideal} are computed by numerical integration methods that are available in the QuTiP package in Python3. For said computation, we use the theoretical driving time τ to perform a perfect π rotation around the x-axis of the Bloch sphere (X-gate). Next, we perform a transformation to the rotating frame of qubit 2 on both propagators by $\tilde{U} = RU$, where $R = \exp(-i\tau\hat{\sigma}_z w_2)$.

Hereafter, we perform a virtual phase correction, done via a virtual Z-gate, on the actual propagator in the rotating frame by performing the transformation $\tilde{U}^* = C\tilde{U}$, where $C = \exp(-i\phi\hat{\sigma}_z)$ for some $\phi \in [0, 2\pi)$ such that the gate fidelity is maximized when substituting $\tilde{U}^*_{actual}$ and $\tilde{U}_{ideal}$ in the gate fidelity equation 2.4. To find the optimal value of ϕ, we use the Nelder-Mead algorithm with $\phi = 0$ as initial guess. A virtual Z-gate can

be easily implemented in the software of a quantum computer [12], and doing a phase correction is necessary since we examine the ideal propagator for a ideal X-gate, which has a known driving time. If we evaluate the actual propagator for some other driving time, we will be off by some phase constant and the gate we have performed could still be the gate we want it to be, only shifted in the (x,y)-plane of the Bloch sphere. By performing a phase correction, we ensure that we get a high fidelity when we drive the correct gate, even if it is off by a phase constant.

3.2. Resonance frequency shift due to heating

To add the heating-induced resonance frequency shift phenomenology to the model, we use experimental data on the dependence of a qubits resonance frequency on the driving time as depicted in figure 3.1. We assume the frequency shift to be due to heating (dielectric and conductive losses), such that the shift depends on the energy P of the driving pulses $f(t) = \frac{\Omega_2}{2}\cos(w_2 t) + \alpha\frac{\Omega_1}{2}\cos(w_1 t)$ in units s^{-1} on qubit 2, given by the formula for time-averaged Joule heating in units of J:

$$P = A \int_0^{t_{drive}} |f(t)|^2 dt \quad ,$$
(3.2)

where A is some constant in units Sm^2 [18]. We have assumed that the pulses $f(t)$ have a rectangular pulse envelope. By curve-fitting the data in figure 3.1 to the function $y = ax^b$, we find that the resonance frequency shift of the qubit depends on the energy of the driving pulses with $\frac{a}{A^b} \approx 8.72*10^{-3} \, skg^{-1}m^{-2}$ and $b \approx 0.292$ as follows:

$$w_{shift} = a\left(\frac{P}{A}\right)^b \quad .$$
(3.3)

We see then that the resonance frequency shift depends on the driving pulse amplitude and the driving time, which adds an extra time-dependent term to the Hamiltonian. The new Hamiltonian is formed by adding the resonance frequency shift to the Larmor frequency of the second qubit in the AC Stark shift Hamiltonian in equation 3.1, leading to the shifted Hamiltonian $H_{2,shift} \in \mathcal{H}_2$:

$$H_{2,shift} = -\frac{w_2 + w_{shift}(t)}{2}\hat{\sigma}_z + \frac{\Omega_2}{2}\cos(w_2 t)\hat{\sigma}_x + \alpha\frac{\Omega_1}{2}\cos(w_1 t)\hat{\sigma}_x \quad .$$
(3.4)

To find the single-qubit gate fidelity for a qubit that suffers from resonance frequency shift, we can follow the method of calculating the gate fidelity described in the section above by replacing H_2 by $H_{2,shift}$.
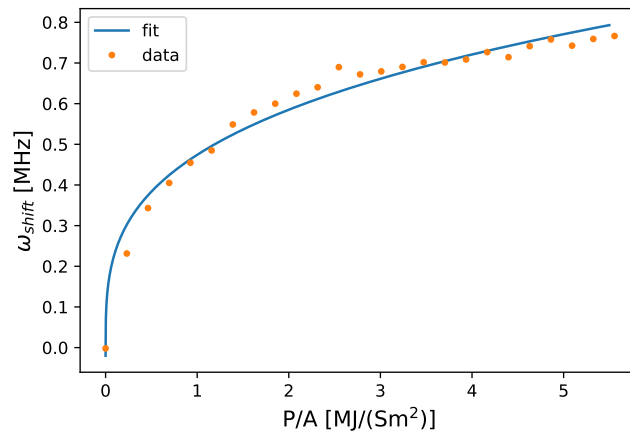
Figure 3.1: Curve-fit of the experimental data of a qubit's resonance frequency shift w_{shift} in MHz as function of the energy P/A, when applying some off-resonant microwave pulse for variable amount of time. The driving time and driving amplitude are converted to units of energy by using formula 3.2 with the factor A incorporated in the curve-fit parameters. The fitted graph is of the form $y = ax^b$ with $\frac{a}{A^b} \approx 8.72*10^{-3} \, skg^{-1}m^{-2}$ and $b \approx 0.292$. The experimental data was obtained during private communications with B.W. Undseth.

3.3. Generalization to multiple drives

Suppose we now want to generalize our model to the case where a single qubit, driven with an X-gate, feels the crosstalk of $M-1$ other drives from other qubits in the total system that are also driven with X-gates. The single-qubit Hamiltonian $H_N \in \mathcal{H}_2$ with $N \leq M$ will now look as follows:

$$H_N = -\frac{w_N}{2}\hat{\sigma}_z + \frac{\Omega_N}{2}\cos(w_N t)\hat{\sigma}_x + \sum_{j=1, j\neq N}^{M} \alpha_j \frac{\Omega_j}{2}\cos(w_j t)\hat{\sigma}_x \quad , \tag{3.5}$$

where w_i and Ω_i for $i = 1, ..., M$ are the resonance frequencies and driving amplitudes (both in rad Hz) of qubits 1 to qubit M respectively. The factor a_j for $j \in \{1, ..., M\} \setminus \{N\}$ represents the amount of influence that qubit N feels of the drives on all other qubits in the system.

If we now add the Larmor frequency shift model into our Hamiltonian, we will get the following Hamiltonian $H_{N,shift} \in \mathcal{H}_2$:

$$H_{N,shift} = -\frac{w_N + w_{shift}(t)}{2}\hat{\sigma}_z + \frac{\Omega_N}{2}\cos(w_N t)\hat{\sigma}_x + \sum_{j=1, j\neq N}^{M} \alpha_j \frac{\Omega_j}{2}\cos(w_j t)\hat{\sigma}_x \quad . \tag{3.6}$$

Again, the only difference with the previous Hamiltonian is the $w_{shift}(t)$ function. The $w_{shift}(t)$ depends on the time and can be calculated by taking $f(t) = \frac{\Omega_N}{2}\cos(w_N t) + \sum_{j=1, j\neq N}^{M} \alpha_j \frac{\Omega_j}{2}\cos(w_j t)$. Since numerical integration of $|f(t)|^2$ takes too long if we afterwards also numerically solve the time-dependent Schrödinger equation to compute the propagator, we solve $\int_0^{t_{drive}} |f(t)|^2 dt$ analytically: assuming $f(t) = \Omega/2 * \sum_{n=1}^{N} \alpha_n \cos(w_n t)$, we can solve $\int_0^{t_{drive}} \sum_{n=1}^{N} \alpha_n \cos^2(w_n t) + 2\sum_{j=1}^{N} \sum_{i=1}^{j-1} \alpha_i \alpha_j \cos(w_i t)\cos(w_j t) dt$ instead.

3.4. Optimization of the gate fidelity

To make silicon quantum computers as useful as possible, we want to obtain the highest possible gate fidelity values. In order to compensate for the AC stark shift and the resonance frequency shift, we investigate if we can find an optimal driving time and driving frequency of qubit N for which we are calculating the single-qubit gate fidelity. The optimization problem that we will be solving is given by

$$\min_{a \leq t_{drive} \leq b, \ c \leq w_{drive} \leq d} -F(t_{drive}, w_{drive})$$
$$s.t. \quad F(t_{drive}, w_{drive}) \leq 1$$
$$-F(t_{drive}, w_{drive}) \leq 0.$$

In the equations above, the function F that depends on the driving time t_{drive} and w_{drive} is given by equation 2.4. The actual propagator is computed from the EDSR Hamiltonian in equation 2.3 and the actual propagator computed from either the AC stark shift Hamiltonian in equation 3.5 or the Hamiltonian including both the AC stark shift and the resonance frequency shift in equation 3.6, by replacing the $cos(w_N t)$ term by $\cos(w_{drive} t)$. For the bounds of the driving time, we take $a = 100$ ns and $b = 500$ ns and for the bounds of the driving frequency we take $c = w_N - 2\pi * 600$ MHz and $d = w_N + 2\pi * 600$ MHz. The driving time bounds include the theoretical driving time t_{theo} (calculated for when we assume there is no crosstalk), which is about 200 ns. The driving frequency bounds are chosen such that the driving frequency is closer to the theoretical driving frequency $w_{theo} = w_N$ than the resonance frequency of a neighbouring qubit. The theoretical driving time and -frequency are the optimal parameters in case we do not take crosstalk into account, since U_{ideal} would be equal to U_{actual} in that case, see section A.1 for more detail.

We solve the above optimization problem using the Nelder-Mead algorithm with t_{theo}, w_{theo} as initial guess. Furthermore, for 2 drives, we perform a brute force grid search for t_{drive} and w_{drive} to investigate how much deviation is permitted from the optimal driving time and -frequency to still obtain 0.99 fidelity. The grid search validates of the optimal parameters found by the Nelder-Mead algorithm, ensuring the algorithm has found a global minimum.

4

Results

In this chapter, we evaluate the model introduced in chapter 3. Following the structure of the previous chapter, we first analyze the AC Stark shift model mentioned in section 3.1. We validate said model in Appendix B by reproducing the results from previous research published in the paper [5]. In the current chapter, we turn to analyzing single-qubit gate fidelities as a function of the driving time and the driving frequency in the presence of two and more drives. We then go on to do the same for the model that includes the resonance frequency shift as mentioned in section 3.2.

4.1. Gate fidelity in the presence of AC Stark shift

4.1.1. Two drives

First, we examine the single-qubit gate fidelities in the presence of AC Stark shift when we apply one on-resonant drive and one off-resonant drive. This is effectively a two-qubit system, where we examine the effect on one of the two qubits. We investigate the effect of applying drives with constant driving amplitude Ω, but with different driving times t_{drive} and different driving frequencies, notated either with w_{drive} in units rad Hz or f_{drive} in units of Hz. We have plotted the grid of gate fidelities in figure 4.1a and we zoomed-in on the high-fidelity values in this figure, which is shown in figure 4.1b. From said figures, we can see that there seems to be a global optimum in the region of $t_{drive}, f_{drive} \approx 200$ ns, 18.693 GHz, which are also the theoretical optimal driving values we use throughout the rest of this chapter when we compare the ideal propagator with the actual propagator, as discussed in section A.1. We may also refer to these theoretical optimal values by t_{theo}, w_{theo}. We proceed to find the optimal driving time and -frequency with the Nelder-Mead algorithm. The calculated optimal values are $t_{drive}, f_{drive} = 200.000281$ ns, 18.6929739 GHz, which differ only slightly from the theoretical values. Whenever we refer to calculated optimal values, we mean optimal values that are a result of the Nelder-Mead algorithm.

4.1.2. Three to six drives

We repeat the same process for up to and including six drives in total. The driving frequencies of the drives differ by a positive or negative integer of a constant value around the resonance frequency of the qubit that we investigate, as shown in figure A.1 in appendix A. We assume this is the case so that the results do not depend on a specific set of resonance frequencies, which limits the parameters we have in our model. The grid searches for all of these drives reveal no significant change as compared to the grid search for the 2 drive case. When plotting the (squared and absolute value of) fidelity difference between 2 and 3 drives in figure 4.2, we notice that there is at most a 0.0003 fidelity difference within a 5 nanosecond and 0.1 MHz window around the theoretical optimum t_{theo}, w_{theo}. This leads us to believe that scaling up the number of drives in the system in the presence of only the AC Stark shift does not change the location of the calculated optimal driving time - and frequency. From figure 4.2a, we can also see that small changes in fidelity appear periodically with a period of slightly less than 5 ns, which is around the order of magnitude of the period of the resonance frequency between the drives $|\Delta f| = 0.2$ GHz. Figure 4.2b also reveals an interesting pattern of lines with minimal fidelity difference, but the difference with the rest of the region in the same figure is 0.00005 fidelity difference, which is minimal.
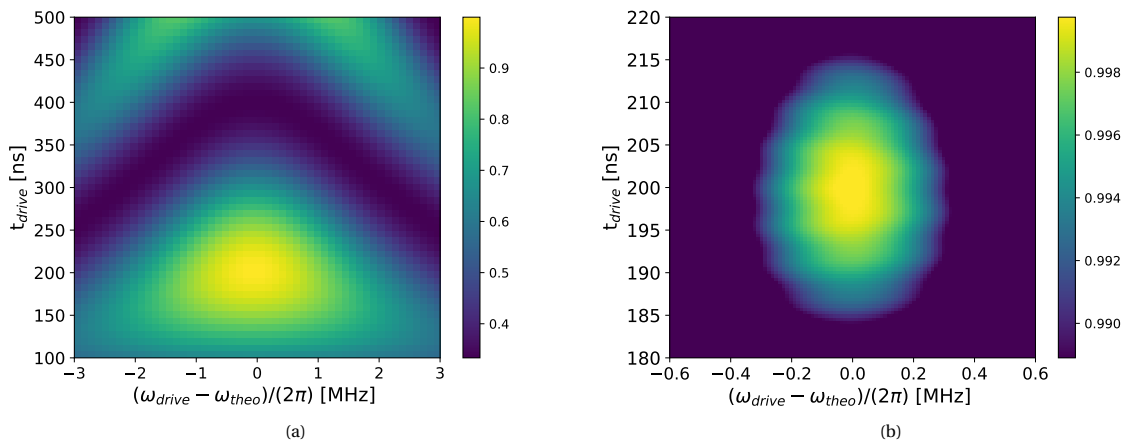
Figure 4.1: Grid of the single-qubit gate fidelity for a qubit being driven with a resonant and off-resonant X-gate. The fidelity is a function of driving time t_{drive} and driving frequency with the theoretical optimal driving frequency $w_{drive} - w_{theo}$. The colorbar represents the gate-fidelity value. Figure **(b)** is zoomed-in on the high-fidelity region in figure **(a)**.
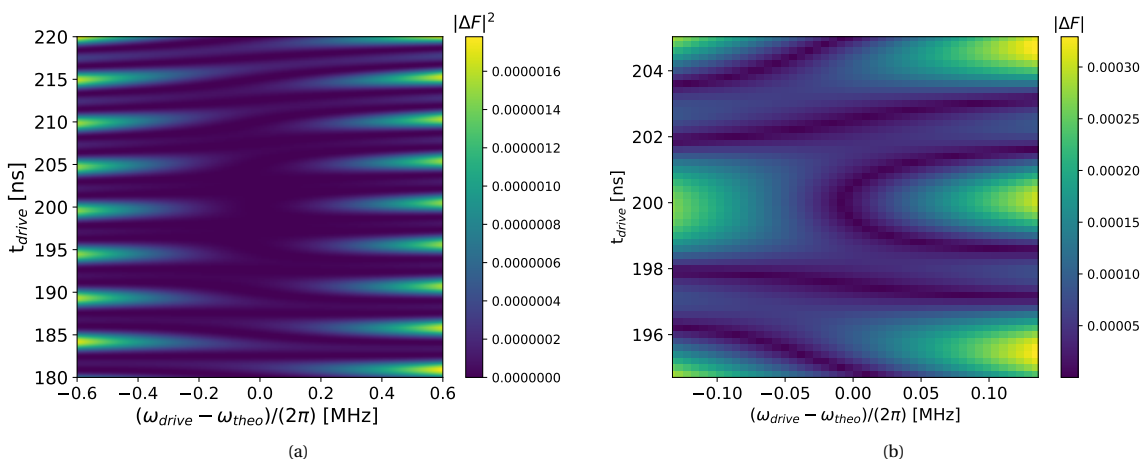
Figure 4.2: Figures of **(a)** the square of the absolute value of the gate fidelity difference between a qubit experiencing effects of 2 or 3 drives and **(b)** showing the region around the theoretical optimal driving time and -frequency: $t = 200$ ns and $(w_{drive} - w_2)/(2\pi) = 0.0$ MHz. Both figures show the gate fidelity as function of driving time and -frequency. We plotted the square of the gate fidelity in the left figure, since the scaling reveals the details we are interested in most clearly.

The hypothesis that scaling up to more drives does not change the optimal parameters meaningfully is further corroborated by the calculated optimal parameters for 2 to 6 drives that take into account the AC Stark shift. The data is visualized in figures 4.3a and 4.3b and the exact data can be found in table C.1 in appendix C. As we can see, the difference in driving time is about 5 orders of magnitude smaller than the theoretical driving time, and the difference in driving frequency is 5 to 6 orders of magnitude smaller than the theoretical driving frequencies. The order of magnitude of the shift $(w_{drive} - w_{theo})/(2\pi)$ also makes sense, since calculation of equation 2.5 for 2 drives gives approximately a 20 kHz resonance frequency shift. Furthermore, we notice in figure 4.3b that for 3 and 5 drives, the absolute frequency difference is zero, which is due to the choice of resonance frequencies for the other qubits. Namely, when we consider the resonance frequency of the qubit of interest for 3 and 5 drives, we have the same drives on the right of this resonance frequency as to the left of this resonance frequency. Figure A.1 in appendix A visualizes this statement more clearly. Furthermore, when we checked if we could also obtain high fidelities when we drive with the theoretical optimal values, we found that we got at least 0.99999 fidelity for 2 to 6 drives (see table C.2 in appendix C for the exact values). This is about the limit of fidelity that can be measured experimentally. Taking everything into account, we conclude that optimization of the driving time and frequency when we just consider the AC Stark shift is not needed to get much higher fidelities.
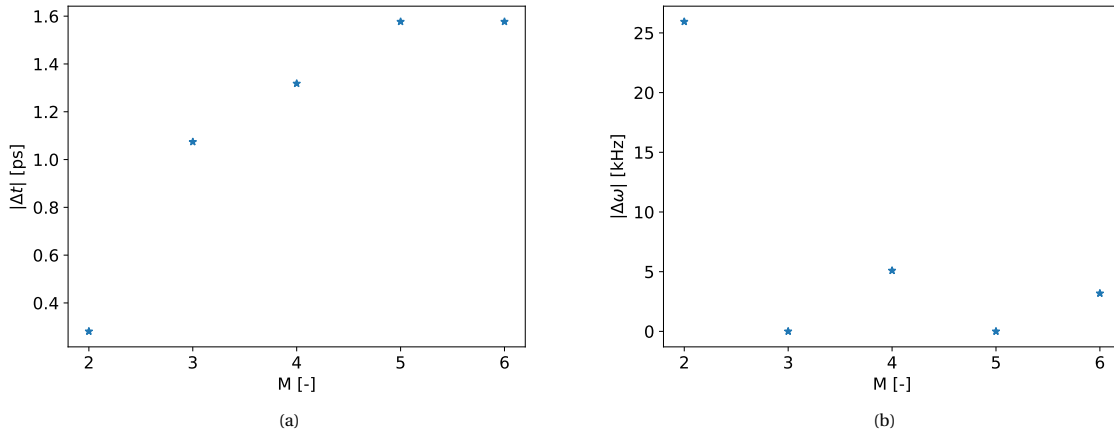
Figure 4.3: Visualization of **(a)** the absolute difference between the theoretical driving time, $\frac{2\pi}{\Omega}$, and the calculated optimal driving time in picoseconds and **(b)** the absolute difference between the theoretical driving frequency, equal to the qubit's resonance frequency w_{theo}, and the calculated optimal driving frequency in kHz. Both differences are plotted as a function of the amount of drives M that we have evaluated the optimal driving time and -frequency for.

4.2. Resonance frequency shift due to heating

So far, we have evaluated what happens when we incorporate AC Stark shift in our model. We now turn our attention to the resonance frequency shift due to the effect of other drives on nearby qubits on the qubit we are interested in.

4.2.1. Heating model

First, to get a clear picture of the time-dependent resonance frequency shift we add to the model, we have examined the resonance frequency shift as a function of driving time for 2 to 6 drives in total, see figure 4.4a. We notice that as we drive for longer, we add more and more resonance frequency shift to the qubit's original resonance frequency, which makes sense because of the function that models the shift (equation 3.3). We also see a constant change between drive 1 and 2, 2 and 3, etc., which is presumably due to the crosstalk factor α of all the off-resonant drives being equal to 0.4 and not 1. In general, we notice that more drives add (slightly) more resonance frequency shift. This is expected since we put more energy into the system. The small oscillations in the graphs are due to the oscillatory behaviour of the pulses. Since the oscillations are so small and the graphs for the several drives diverge from one another, the effect of the oscillations can be ignored for driving times larger than a hundred nanoseconds since the graphs do not overlap anymore.

If we now plot the single-qubit gate fidelities for the heating model when driving them at the theoretical optimal driving time $t_{drive} = t_{theo}$ ns and $w_{drive} = w_{theo}$ in figure 4.4b, we can see that the fidelities have significantly decreased in comparison to the earlier near-perfect fidelities that we calculated for the same values using the model discussed in the previous section. Furthermore, we note that the fidelity appears to decrease linearly as a function of the amount of drives coupled to the qubit. This implicates that the resonance frequency shift is a serious problem for currently existing quantum processors (which have up to 6 qubits) since it affects the fidelities by 33 percent. What's more, is that this linear decrease implies that the resonance frequency shift will become a larger problem in terms of fidelity when quantum processors are scaled to more qubits and we do not correct for the resonance shift.

4.2.2. Two drives

In order to find a way to correct for this significant decrease in fidelity, we proceed to evaluate the single-qubit gate fidelities in the resonance frequency shift model as a function of the driving time and the driving frequency in the same way as in the previous section. We have plotted the grid of gate fidelities in figure 4.5a and we zoomed-in on the high-fidelity values in this figure, which is shown in figure 4.5b. When comparing these figures with the same figures from before (figures 4.1a, 4.1b), we can see that the patterns on the larger grids are almost the same, but that the pattern in figure 4.5a has slightly shifted to the right and has stretched with respect to the frequency axis and it appears to tilt slightly to the top-right corner. For the resonance frequency shift model, there still appears to be a global optimum around the theoretical driving time, but the

13
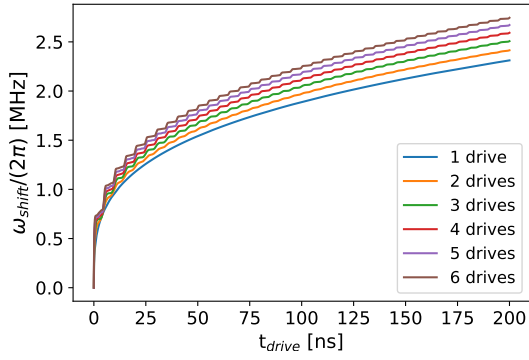
(a) Graphs of the resonance frequency shift in MHz as function of the driving time t_{drive} up to the theoretical driving time t_{theo} for 1 to 6 drives with crosstalk factor $\alpha = 1$ for the on-resonance drive and $\alpha = 0.4$ for all the other drives. The driving frequency w_{drive} is assumed to be equal to the theoretical driving frequency w_{theo}. The small oscillations in the graphs are due to the oscillatory behaviour of the driving pulses. The graph shows that the shift is much larger than the shift on which we curve-fitted the model (figure 3.1, but this is due to using higher driving strength, which makes it logical that the energy and thus the resonance frequency shift is also higher.
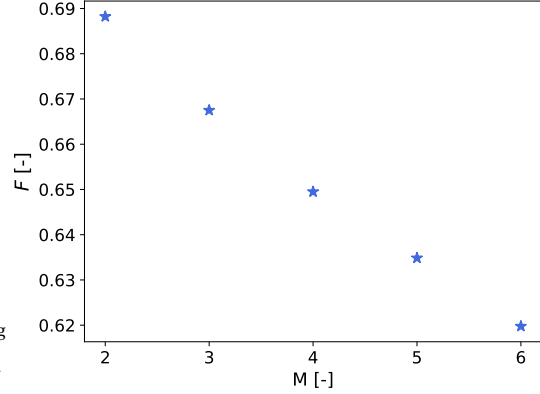
(b) Data of the single-qubit gate fidelities F as function of the number of drives M that are coupled to the qubit, calculated for the resonance frequency model when taking the driving time and -frequency to be equal to the theoretical optimal values t_{theo} and w_{theo}. The fidelity seems to linearly decrease when adding more drives.

Figure 4.4

optimal driving frequency seems to shifted along with the grid pattern by about 2 MHz. The tilt to the top-right corner of the figure can be explained by a higher resonance frequency shift due to a longer driving time.

Again, we proceed to find the optimal driving time and -frequency with the Nelder-Mead algorithm. The calculated optimal values are t_{drive}, f_{drive} = 200.66 ns, 18.694927215 GHz, which differ by approximately 0.66 ns and 1.93 MHz from the theoretical optimal values. These values are significantly larger than the values found in section 4.1.1. Furthermore, we see from figure 4.5b that > 0.99 fidelity range is about the same as for only AC Stark shift: 0.2 MHz and 15 ns around the calculated optimum. However, In terms of percentages, these ranges are approximately 0.0002 % and 7.5% of w_{theo} and t_{theo}, respectively. Furthermore, the calculated optimal driving time still lies within the 15 ns range from the theoretical optimum, so by driving at the theoretical optimal driving time, we can still get more than 0.99 fidelity, whereas it is clear that when we incorporate a resonance frequency shift due to heating, we do not obtain high-fidelities anymore. Both the ranges to get 0.99 fidelity and the fact that the theoretical driving time is still within this range, suggest that for obtaining high fidelities, it is most important to focus on finding the optimal driving frequency and much less important to find the optimal driving time.
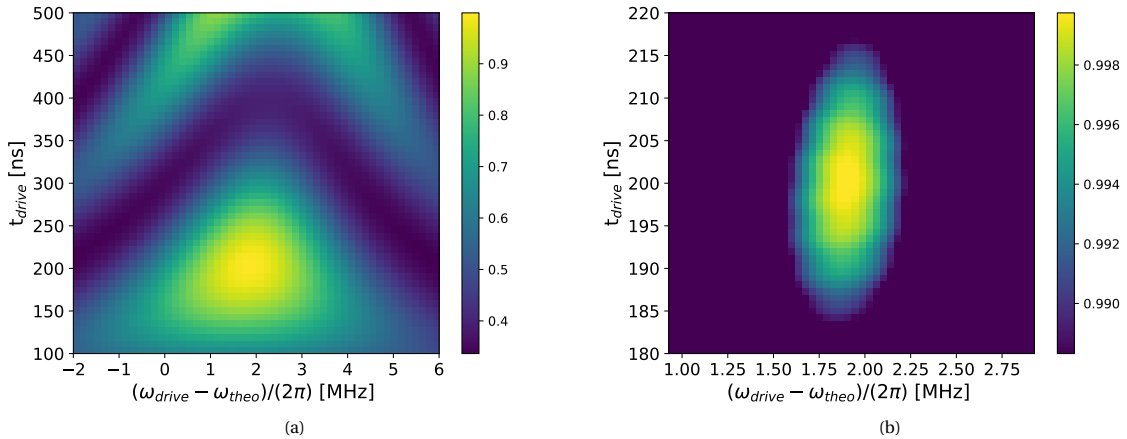
Figure 4.5: Grid of the single-qubit gate fidelity for a qubit being driven with a resonant and off-resonant X-gate. The fidelity is a function of driving time t_{drive} and driving frequency w_{drive}. The colorbar represents the gate-fidelity value. Figure **(b)** is zoomed-in on the high-fidelity region in figure **(a)**.

4.2.3. Three to six drives

We also investigate what happens to the optimal driving time and -frequency when we add more drives that couple to the qubit. The parameters that are used for these extra drives are exactly the same as used for the results of the previous model. Again we plot the absolute difference in driving time and the absolute difference in driving frequency with respect to the theoretical optimum in figures 4.6a and 4.6b, respectively. From said figures, we can see that the optimization yields about a 1% difference in terms of driving time and about a 0.002% difference in driving frequency with respect to the theoretical optimum. The data is included in table C.3 in appendix C, and from this data we note that the optimized fidelity gives us at least 9 digits of 9 fidelities again, implicating that we can completely correct for the heating-induced resonance frequency shift by optimization of the driving time and -frequency. From figure 4.6b, we also note that the difference in driving frequency seems to approximately linearly depend on the amount of drives coupling to the qubit. The plotted orange line is given by the function $\Delta w = aM + b$, where Δw is the absolute frequency difference, M is the number of drives, a = 0.066575 MHz/drive and b = 1.80 MHz. We also do not see a drop in the difference of the driving frequency and the theoretical driving frequency for odd drives as we did previously. This is because the resonance frequency shift is mainly caused by the energy of the drives and not so much the frequency of the drives. Furthermore, since the resonance frequency shift has a much larger impact on the resonance frequency than the AC Stark shift, the symmetry of the odd amount of drives around the qubit's resonance frequency is broken.
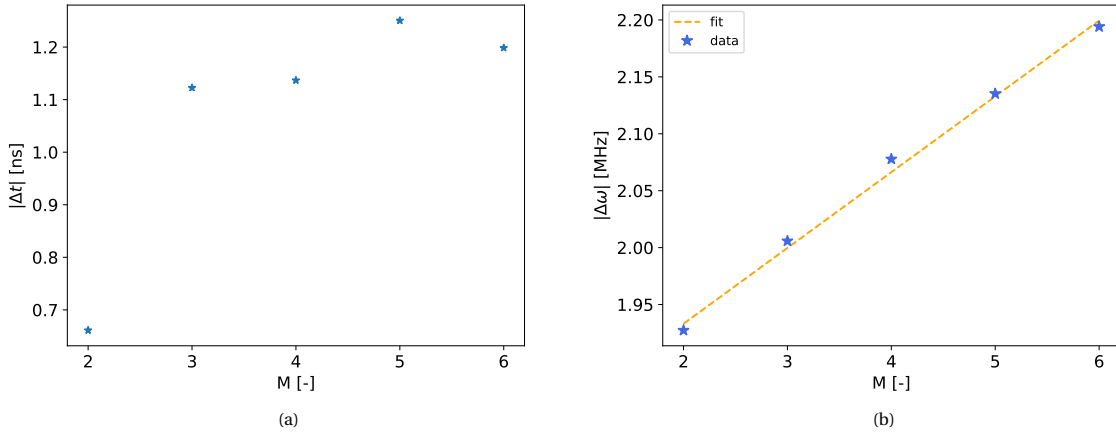
Figure 4.6: Visualization of **(a)** the absolute difference between the theoretical driving time, $\frac{2\pi}{\Omega}$, and the calculated optimal driving time in picoseconds and **(b)** the absolute difference between the theoretical driving frequency w_{theo} and the calculated optimal driving frequency in MHz when there is a resonance frequency shift. Both differences are plotted as a function of the amount of drives M that we have evaluated the optimal driving time and -frequency for. The dashed orange line shows that the relation between the absolute driving frequency difference and the number of drives is almost linear. The corresponding data is included in table C.3 in appendix C.

If we now plot the resonance frequency shift of the qubit at the theoretical driving time t_{theo} and the data displayed figure 4.6b together in figure 4.7, we learn that the relation of the resonance frequency shift at the theoretical driving time and the optimal calculated driving frequency are very similar, and differ by about 0.5 MHz. The spacing between the heating-induced resonance frequency shift and the driving frequency correction is presumably caused by the time-dependence of the heating term, and by the capacitive gate coupling term that was already included in the first model. Since we only have a limited set of data points (5 data points), further research efforts can go into repeating the same steps, but for more than six drives. Despite the small amount of data available on which the 0.5 MHz difference has been found, it could provide a rough estimate on what driving frequency could offer higher gate fidelities should the we know the resonance frequency shift in advance.
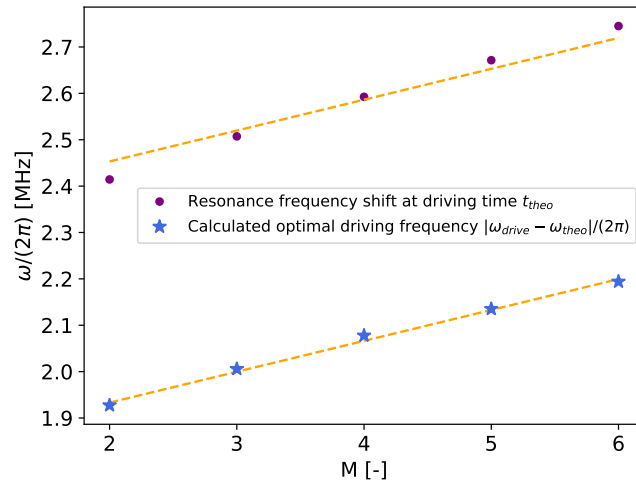
Figure 4.7: The blue stars visualize the absolute difference between the theoretical driving frequency, equal to the qubit's resonance frequency w_{theo}, and the calculated optimal driving frequency in MHz when there is a resonance frequency shift (blue). The purple dots show the resonance frequency shift $w_{shift}/(2\pi)$ of the qubit at a driving time t_{theo}. Both are plotted as a function of the number of drives M. The dashed orange lines shows that the relation between the absolute driving frequency difference and the number of drives is almost linear. The absolute difference between the two lines is 0.52 MHz.

5

Discussion

In this chapter we discuss assumptions and limitations of the model and the way it is programmed into Python3. Then, we give recommendations for driving gates on qubits that are resonance frequency shifted. Finally, we provide suggestions for further research.

5.1. Model

First, we assumed that extra resonance frequency shift in the second model is due to the heating effect caused by the AC electromagnetic fields that are driving the quantum gates on the qubits. There may be other (unknown) electromagnetic wave-induced effects going on here that are not considered. The curve-fit that determines the dependence of the resonance frequency shift on the energy of the driving pulses is based on a single data set. The dependence of the pre-factor A in formula 3.2 is absorbed into the factor a in equation 3.3, and this factor is assumed to be constant for all drives we add to the system.

Secondly, we saw from figure 4.4a that the longer we drive the qubit, the more the resonance frequency will shift. We only aimed to drive a single gate with high-fidelity, but for scalable quantum computing the gate fidelities must remain high for driving multiple qubit gates after one another. Since we modelled this effect as heating, this heating and thus the frequency shift will build up when gates or multiple gates are driving for longer. Driving longer might lower fidelities significantly if we do not correct for this shift. Instead of correcting for the shift, one could also allow the qubits to cool down after every operation to keep the resonance frequency shift as low as possible. Of course, cooling time would significantly decrease the speed at which the quantum computers can perform operations, which could defeat the purpose of a quantum computer.

We have also assumed that the crosstalk factor α is the same for all drives on other qubits. We expect that this assumption does not hold for large 1D qubit arrays or other large 2D qubit arrays. Namely, localized microwave pulses on one qubit located far away from a qubit will not impact as much as the effect a neighbouring driven qubit. A possibility is to consider the middle most qubit of the qubit array such that the effects of crosstalk are symmetric and/or let α decrease for qubits further away from the qubit we investigate.

On the design of the slanting magnetic field that gives the qubits an individual resonance frequency, we also saw that for odd drives, the AC Stark shift is minimal. Suppose the resonance frequencies can be engineered precisely so that each qubit differs by the same amount in resonance frequency. In that case, we can minimize the effect of AC Stark shift on single-qubit gates by the design of the slanting magnetic field.

As discussed in section B.1 the choice of driving strength Ω for each drive can also impact the gate-fidelities, since the different driving strengths affect the detuning of a qubit's Rabi frequency. The driving strength Ω is chosen to be equal for all drives, for the reasons discussed in section B.1, but one could investigate how different driving strengths for other drives impact the fidelity the qubit's whose resonance frequency is shifted. By equation 3.2, we expect that the driving strength Ω will have a significant impact on the resonance frequency shift on the qubit.

Another issue encountered in this project is the sensitivity of the numerical integration methods used to calculate the propagators. The default settings of the relative tolerance bounds were already limiting the accuracy of the results for two drives without resonance frequency shift. We have solved this issue by decreasing the values for both the absolute and relative tolerance until decreasing further did not alter the fidelity results. We proceeded to work with a relative and absolute tolerance of 1e-14 and 1e-13 respectively. In the grid searches

done for more drives, using these tolerance settings resulted in continuous patterns, which leads us to believe that any further decrease of tolerance settings is unnecessary and would only increase computation time.

5.2. Recommendations for experimental quantum computing in silicon

Based on the results, the effect of just the AC Stark shift on the single-qubit gate fidelities is negligible. Namely, we still obtain very high fidelities and, optimization in terms of driving frequency and driving time only gives a minimal improvement at the limit of what is measurable in experiments. However, when an extra resonance frequency is added on top of the AC Stark shift, we have seen that we need to take the crosstalk into account when we want to obtain high fidelities. Experimental research efforts should get conclusive proof that this extra resonance frequency shift is indeed due to heating caused by the energy that the drives feed into the quantum system. The resonance frequency as an effect of heating suggests that over longer driving times and for driving more qubits, the shift will get larger and decrease fidelities further. This shift can be lowered by ensuring the system has enough time to cool down after driving and/or it can be corrected by optimizing the driving parameters. In terms of driving parameters, the driving frequency of the single qubit we evaluate the fidelity of matters a lot, but the driving time is expected to matter less. In addition, the driving strength Ω has a lot of impact on the energy we supply into the system, as discussed earlier in this chapter. We expect that keeping the driving strength minimal and optimizing the driving frequency should already give much higher fidelities. For optimization of single-qubit gate fidelities in presence of other drives, using the model that is presented in this thesis should provide an indication for the optimal driving frequency. Furthermore, the relationship between the resonance frequency shift at the theoretical driving time and the optimal frequency shift should be investigated further for more drives. If the 0.5 MHz difference between the two holds, it is expected that it provides an easy way to achieve high gate fidelities if the heating-induced resonance frequency shift is known.

5.3. Suggestions for further research

Because of long computation time (even when running the code in parallel), it was not possible to generate data for more than 6 drives with resonance frequency added within the time-frame of this project. For further research, we'd recommend generating data for more than six drives. More data-points will give more insight into the dependence of the resonance frequency shift and the optimal driving values and one might gain valuable insights from this.

For this project we have assumed that qubits are uncoupled and that they therefore undergo no qubit-qubit interactions. Further research can include qubit-qubit coupling and see how the results change. Researching this is vital since universal high-fidelity quantum computing relies on the performance of a set of both single-qubit and two-qubit gates. This set of gates should at least include some entangling gate such as the Controlled NOT-gate, CNOT, which can entangle and disentangle qubits and all of the two-qubit gates, such as the CNOT gate, rely on having the qubit-qubit interactions turned on instead of off. [1] Therefore, adding qubit-qubit interactions to the model and evaluating the fidelities of two-qubit gates is suggested for further research.

Moreover, reliable quantum computers depend on the single-qubit gate fidelity, but also on the fidelity of the whole system. To get the whole picture on how the crosstalk (AC Stark- and the extra resonance frequency shift) affect the fidelity of a quantum computer, one should investigate this 'whole system' fidelity. We can extract these fidelities for uncoupled qubits by taking the tensor product of all the single-qubit Hamiltonians and computing the propagator. Note that the dimension of the Hilbert space will then scale with 2^M for M qubits in the total system, presumably making the calculations a lot heavier on the computer and thus data generation will take much longer. For coupled qubits, one cannot simply take the tensor product of the single-qubit Hamiltonians, since the qubit-qubit interactions will add additional terms to the whole system Hamiltonian.

6

Conclusion

When including the AC Stark shift to the effective ESDR Hamiltonian, we can still obtain single-qubit fidelities higher than 0.99999 even if we do not correct for the crosstalk. This lower bound for the fidelity is already very high, and it is at the limit of the fidelity that can be measured experimentally at the moment, which means that we could ignore the AC Stark shift when it is the only crosstalk that works on the qubits. However, should even higher fidelities be preferred, one could change the driving time and driving frequency in ps and kHz range respectively from the theoretical optimal driving parameters, calculated for when we do not take crosstalk into account. When hitting the optimum, fidelities are higher than 10 digits of 9.

With our heating model, we compute resonance frequency shifts from 2.3 to 2.7 MHz for two to six drives, respectively. Adding this shift on top of the AC Stark shift, we get at most 0.69 fidelity when we drive at the theoretical optimal parameters that do not consider crosstalk. Furthermore, we see a linear decrease in the fidelity when we add more drives that influence the qubit. Thus, to realize scalable silicon quantum computers while maintaining high fidelities, it is very important to consider the resonance frequency shift as an effect of heating. We find that we can correct for the decreasing fidelity by optimizing the driving time and -frequency in the ns and MHz range, resulting in at least nine digits of 9 fidelity. For all drives, the correction that we perform on the theoretical optimal driving values is much higher for the driving frequency than for the driving time (1% and 0.002%, respectively), which implies that we can get the most fidelity gain from finding the optimal driving frequency. The range for getting at least 0.99 fidelity is about 0.2 MHz around the optimal driving frequency for two drives. Furthermore, we discover that there is a linearly increasing dependence of the resonance frequency shift at the theoretical driving time as a function of the total drives. Up to a translation factor of 0.5 MHz, we notice the same linear relationship for the correction needed on the theoretical driving frequency to hit maximum fidelity as a function of the total drives. Due to the lack of a large data set for said relationship, we suggest investigating this relationship more closely in further research. Evaluating multiple-qubit gate fidelity and whole system fidelity is also left for further research, which is important for forming the entire picture of how AC Stark shift combined with heating-induced resonance frequency shift affects a silicon quantum computer.

Bibliography

[1] Adriano Barenco, Charles H. Bennett, Richard Cleve, David P. DiVincenzo, Norman Margolus, Peter Shor, Tycho Sleator, John A. Smolin, and Harald Weinfurter. Elementary gates for quantum computation. *Physical Review A*, 52(5):3457–3467, nov 1995. doi: 10.1103/physreva.52.3457. URL `https://doi.org/10.1103%2Fphysreva.52.3457`.

[2] Nikesh S. Dattani. Linear multistep numerical methods for ordinary differential equations, 2008. URL `https://arxiv.org/abs/0810.4965`.

[3] Solomon Freer, Stephanie Simmons, Arne Laucht, Juha T Muhonen, Juan P Dehollain, Rachpon Kalra, Fahd A Mohiyaddin, Fay E Hudson, Kohei M Itoh, Jeffrey C McCallum, et al. A single-atom quantum memory in silicon. *Quantum Science and Technology*, 2(1):015009, 2017.

[4] David J Griffiths and Darrell F Schroeter. *Introduction to quantum mechanics*. Cambridge university press, 2018.

[5] Irina Heinz and Guido Burkard. Crosstalk analysis for single-qubit and two-qubit gates in spin qubit arrays. *Phys. Rev. B*, 104:045420, 07 2021. doi: 10.1103/PhysRevB.104.045420. URL `https://link.aps.org/doi/10.1103/PhysRevB.104.045420`.

[6] Peng Jiang, Yingrui Yang, Gann Bierner, Fengjie Alex Li, Ruhan Wang, and Azadeh Moghtaderi. Ranking in genealogy: Search results fusion at ancestry, 2019. URL `https://arxiv.org/abs/1903.00099`.

[7] Remie Janssen Karen Aardal, Leo van Iersel. *Lecture Notes AM2020 Optimization*. Faculty of EEMCS, TU Delft, 2020.

[8] Phillip Kaye, Raymond Laflamme, and Michele Mosca. *An introduction to quantum computing*. OUP Oxford, 2006.

[9] Jeffrey C Lagarias, James A Reeds, Margaret H Wright, and Paul E Wright. Convergence properties of the nelder–mead simplex method in low dimensions. *SIAM Journal on optimization*, 9(1):112–147, 1998.

[10] Daniel Loss and David P. DiVincenzo. Quantum computation with quantum dots. *Phys. Rev. A*, 57:120–126, Jan 1998. doi: 10.1103/PhysRevA.57.120. URL `https://link.aps.org/doi/10.1103/PhysRevA.57.120`.

[11] Eugene S Mananga and Thibault Charpentier. Introduction of the floquet-magnus expansion in solid-state nuclear magnetic resonance spectroscopy. *The Journal of chemical physics*, 135(4):044109, 2011.

[12] David C. McKay, Christopher J. Wood, Sarah Sheldon, Jerry M. Chow, and Jay M. Gambetta. Efficient mml:math xmlns:mml="http://www.w3.org/1998/math/MathML"mml:miz/mml:mi/mml:math gates for quantum computing. *Physical Review A*, 96(2), aug 2017. doi: 10.1103/physreva.96.022330. URL `https://doi.org/10.1103%2Fphysreva.96.022330`.

[13] John A Nelder and Roger Mead. A simplex method for function minimization. *The computer journal*, 7(4):308–313, 1965.

[14] Michael A Nielsen and Isaac Chuang. Quantum computation and quantum information, 2010.

[15] Line Hjortshøj Pedersen, Niels Martin Møller, and Klaus Mølmer. Fidelity of quantum operations. *Physics Letters A*, 367(1-2):47–51, 2007.

[16] Stephan G. J. Philips, Mateusz T. Mądzik, Sergey V. Amitonov, Sander L. de Snoo, Maximilian Russ, Nima Kalhor, Christian Volk, William I. L. Lawrie, Delphine Brousse, Larysa Tryputen, Brian Paquelet Wuetz, Amir Sammak, Menno Veldhorst, Giordano Scappucci, and Lieven M. K. Vandersypen. Universal control of a six-qubit quantum processor in silicon, 2022. URL `https://arxiv.org/abs/2202.09252`.

[17] M Pioro-Ladriere, T Obata, Y Tokura, Y-S Shin, Toshihiro Kubo, K Yoshida, T Taniyama, and S Tarucha. Electrically driven single-electron spin resonance in a slanting zeeman field. *Nature Physics*, 4(10):776–779, 2008.

[18] David M Pozar. *Microwave engineering*. John wiley & sons, 2011.

[19] S.E. Rasmussen, K.S. Christensen, S.P. Pedersen, L.B. Kristensen, T. Bækkegaard, N.J.S. Loft, and N.T. Zinner. Superconducting circuit companion—an introduction with worked examples. *PRX Quantum*, 2 (4), dec 2021. doi: 10.1103/prxquantum.2.040204. URL https://doi.org/10.1103%2Fprxquantum.2.040204.

[20] K Takeda, J Yoneda, T Otsuka, T Nakajima, MR Delbecq, G Allison, Y Hoshi, N Usami, KM Itoh, S Oda, et al. Optimized electrical control of a si/sige spin qubit in the presence of an induced frequency shift. *npj Quantum Information*, 4(1):1–6, 2018.

[21] Brennan Undseth, Xiao Xue, Mohammad Mehmandoost, Maximilian Russ, Nodar Samkharadze, Amir Sammak, Viatcheslav V. Dobrovitski, Giordano Scappucci, and Lieven M. K. Vandersypen. Nonlinear response and crosstalk of strongly driven silicon spin qubits, 2022. URL https://arxiv.org/abs/2205.04905.

[22] B.W. Undseth. Private communications, 2022.

[23] L. M. K. Vandersypen, H. Bluhm, J. S. Clarke, A. S. Dzurak, R. Ishihara, A. Morello, D. J. Reilly, L. R. Schreiber, and M. Veldhorst. Interfacing spin qubits in quantum dots and donors—hot, dense, and coherent. *npj Quantum Information*, 3(1), sep 2017. doi: 10.1038/s41534-017-0038-y. URL https://doi.org/10.1038%2Fs41534-017-0038-y.

[24] T. F. Watson, S. G. J. Philips, E. Kawakami, D. R. Ward, P. Scarlino, M. Veldhorst, D. E. Savage, M. G. Lagally, Mark Friesen, S. N. Coppersmith, M. A. Eriksson, and L. M. K. Vandersypen. A programmable two-qubit quantum processor in silicon. *Nature*, 555(7698):633–637, 02 2018. doi: 10.1038/nature25766. URL https://doi.org/10.1038%2Fnature25766.

[25] Margaret H Wright. Direct search methods: Once scorned, now respectable. *Pitman Research Notes in Mathematics Series*, pages 191–208, 1996.

[26] X. Xue, T. F. Watson, J. Helsen, D. R. Ward, D. E. Savage, M. G. Lagally, S. N. Coppersmith, M. A. Eriksson, S. Wehner, and L. M. K. Vandersypen. Benchmarking gate fidelities in a Si/SiGe two-qubit device. *Phys. Rev. X*, 9:021011, 04 2019. doi: 10.1103/PhysRevX.9.021011. URL https://link.aps.org/doi/10.1103/PhysRevX.9.021011.

[27] Daniel Zeuch, Fabian Hassler, Jesse J Slim, and David P DiVincenzo. Exact rotating wave approximation. *Annals of physics*, 423:168327, 2020.

[28] Floris A. Zwanenburg, Andrew S. Dzurak, Andrea Morello, Michelle Y. Simmons, Lloyd C. L. Hollenberg, Gerhard Klimeck, Sven Rogge, Susan N. Coppersmith, and Mark A. Eriksson. Silicon quantum electronics. *Reviews of Modern Physics*, 85(3):961–1019, jul 2013. doi: 10.1103/revmodphys.85.961. URL https://doi.org/10.1103%2Frevmodphys.85.961.

[29] AMJ Zwerver, T Krähenmann, TF Watson, Lester Lampert, Hubert C George, Ravi Pillarisetty, SA Bojarski, Payam Amin, SV Amitonov, JM Boter, et al. Qubits made by advanced semiconductor manufacturing. *Nature Electronics*, 5(3):184–190, 2022.

Parameters

In the following table, we introduce the values of all parameters that are introduced in Chapter 3.

Table A.1: Table containing all the parameters of Chapter 3 and corresponding values that were used to generate data. As said before, we take $\hbar = 1$.

Parameter	Meaning of parameter	Value	Unit
w_1	Resonance/Larmor frequency of the first qubit in the system	$2\pi * 18.493$	rad GHz
Δw	Frequency difference between the resonance frequencies of neighbouring qubits	$2\pi * 0.2$	rad GHz
w_j	$j \in \{1,...M\}$. Resonance/Larmor frequencies of all qubits in the system, where M signifies the last qubit.	see figure A.1	rad GHz
Ω_j	$j \in \{1,...M\}$. Driving amplitude of the quantum gates that are performed on the system. Choice of driving amplitude is explained in section B.1.	$2\pi * 5$	rad MHz
d	Dimension of the Hilbert space of the Hamiltonian and Propagator for a single qubit.	2	-
α_j	$j \in \{1,...M\} \setminus \{N\}$. Crosstalk factor, symbolizing how much influence the drives of quantum gates have on the single-qubit that we are interested in	0.4	-
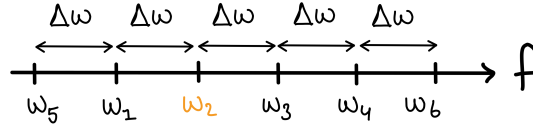
Figure A.1: Resonance frequencies of the different drives used for in this project. We examine the effects of the drives on the single-qubit gate fidelity of the qubit in orange with resonance frequency shift w_2.

A.1. Theoretical optimal driving time and -frequency

Here we provide the derivation of the theoretical optimal driving time and frequency. Said theoretical values are determined for the assumption that there is no crosstalk present in the system, so H_{actual} does not contain crosstalk terms anymore and is equal to

$$H_2 = -\frac{w_{drive}}{2}\hat{\sigma}_z + \frac{\Omega_2}{2}\cos(w_2 t)\hat{\sigma}_x \quad , \tag{A.1}$$

where all parameters are as defined in chapter 3. The ideal Hamiltonian H_{ideal} is the same as the EDSR Hamiltonian in equation 2.3 and we use the theoretical driving time τ to perform a perfect π rotation around the x-axis of the Bloch sphere (X-gate), as discussed in chapter 2 and 3. By comparing both equation 2.3 and A.1, we note that the time evolution operators of both of the Hamiltonians can only be equal when $w_{drive} = w_2$ (or equal to w_N when we consider multiple drives) and $t_{drive} = \tau$. Naturally, for two equal time evolution operators, the fidelity is equal to one, which is the optimal fidelity that one can achieve:

$$F(\tau) = \frac{d + |\text{Tr}[U_{ideal}^{\dagger}(\tau)U_{actual}(\tau)]|^2}{d(d+1)}$$

$$= \frac{2 + |\text{Tr}[U_{ideal}^{\dagger}(\tau)U_{ideal}(\tau)]|^2}{2(2+1)} = \frac{2 + |\text{Tr}[I]|^2}{2(2+1)} = \frac{2 + |2|^2}{6} = 1. \quad \blacksquare$$

B

Validation of AC Stark shift model

To validate the AC Stark shift model mentioned in section 3.1, we reproduced the results from previous research published in [5]. Their research was done by using approximations such as the Rotating Wave Approximation for a single drive and the Floquet Magnus Expansion for two drives to extract the propagators of interest, whereas this project uses the numerical tools that the QuTiP package in Python3 offers to extract the propagators. The reason for using the numerical tools is the minimization of approximation errors and ease of scaling up the drives affecting a single qubit.

All parameters used throughout this project are the same as the parameters used for the results of the research we aimed to reproduce. The results of this reproduction are presented in figures B.1 and B.2. The blue line in figure B.1 seems to reproduces the blue line in figure 2b of the article [5] quite accurately. The orange line (overlapping the blue line) in figure B.1 represents the gate fidelity computed by using the numerical tools in the QuTiP package. As the blue and orange lines overlap, we have corroboration that the programmed AC Stark shift model for a single drive on an idling qubit is corroborated.

Figure B.2 aims to reproduce figure 5 of article [5]. From comparing these two figures, we see that these seem to overlap quite accurately too. Note that to reproduce the results accurately, the tolerance bounds of the numerical integration methods had to be increased as compared to the tolerance bounds used to generate the data of the orange line in figure B.1. Again, we have more corroboration for assuming the AC Stark shift model is correct.
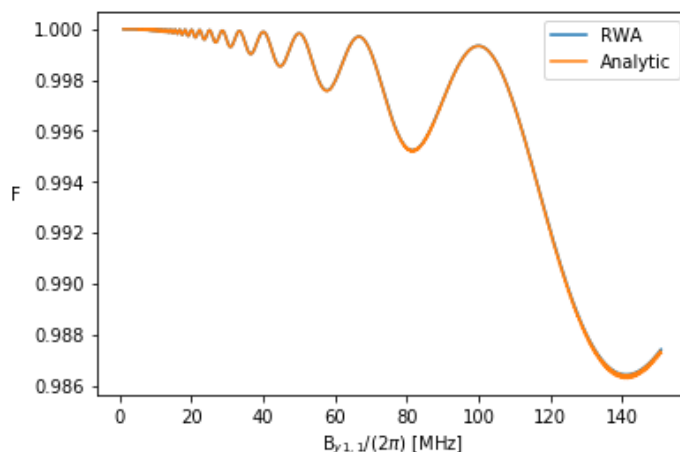
Figure B.1: Gate fidelity of an idling qubit in the presence of a qubit being driven with a Y-gate closeby. The resulting drive on the qubit in question is off-resonant. The crosstalk factor α is 0.4. The single-qubit gate fidelity is plotted as a function of the driving strength $B_{y,11}$ of the Y-gate that's being driven on another qubit. The driving strength $B_{y,11}$ uses the same notation as in the article [5], but it is equal to Ω_1 in the notation used throughout this project. The blue represents fidelity calculated with the effective EDSR Hamiltonian in equation 2.3 as H_{actual} and the orange line shows the fidelity calculated from the numerically calculated propagators.
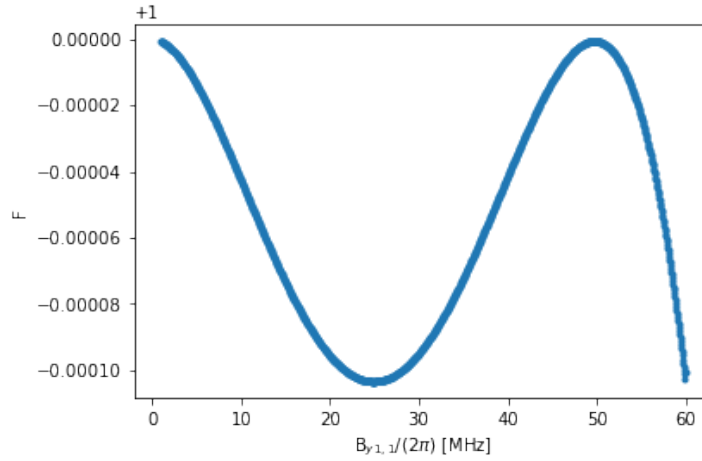
Figure B.2: Gate fidelity of a qubit driven with a Y-gate in the presence of another qubit being driven with a Y-gate. The crosstalk factor α is 0.4. The qubit in question now feels both resonant and off-resonant drives. The single-qubit gate fidelity is plotted for one qubit as function of the driving strength $B_{y,11}$ of the Y-gate that's being driven on the other qubit. The driving strength $B_{y,11}$ uses the same notation as in the article [5], but it is equal to Ω_1 in the notation used throughout this project. The driving strength Ω_2 used here is $5 * 2\pi$ MHz. The blue represents gate fidelity calculated with the numerically calculated propagators.

B.1. Synchronization condition

A result that follows directly from the two figures is that the driving strength we use to drive our qubits with impacts the fidelity a lot. A way to optimize the gate-fidelities is to ensure the driving strengths of the several drives working on the qubit follow the synchronization condition [5]. For idling qubits in the presence of a single other off-resonant drive, the synchronization condition returns us the local maxima of the graphs in figure B.1. For a driven qubit with a single other off-resonant drive nearby, the synchronization condition gives us the local maxima of the graphs figure B.2. However, the end-goal of this project is to investigate effects of resonance frequency shift on single-qubit gate fidelities, and the synchronization condition assumes that the drive on the qubit of interest in on-resonance. We are unsure how this extra off-resonance drive changes the analytical synchronization condition. We expect that in the presence of the resonance frequency shift, we will have an effective off-resonant drive that is the sum of the two drives, since the drives are both X- or Y-gates. The plot in figure B.1 then gives us the most information about which driving strength to use for driving the qubits. From the figure we see that for $B_{y,11}/2\pi \lesssim 10$ MHz oscillations in the gate fidelity are minimal. Therefore, we choose to drive all of our gates with a driving strength that is beneath this bound, namely $B_y/2\pi = \Omega/2\pi = 5$ MHz. Another reason for choosing a low driving strength is that it easier to use a lower driving strength in laboratory experiments.

C

Data

Here we put all the exact data values that are visualized in the results section.

Table C.1: Table showing the theoretical and optimized driving time t_{drive} and driving frequency w_{drive} for different drives in the AC Stark model (no resonance frequency shift due to heating) and their difference with the idealized case, 200 ns and $1.17451582e11$ rad Hz respectively. We also give the rounded fidelity at the calculated optimal driving time and -frequency.

Drives	Optimal t_{drive} [s]	$\lvert t_{drive} - t_{id}\rvert$ [ps]	Optimal w_{drive} [rad Hz]	$\lvert w_{drive} - w_{id}\rvert$ [kHz]	F
2	2.00000281e-07	0.281	1.17451419e+11	25.94225572	0.99999999997
3	1.99998926e-07	1.074	1.17451582e+11	0	0.99999999998
4	1.99998682e-07	1.318	1.17451614e+11	5.09295818	0.999999999999
5	1.99998423e-07	1.577	1.17451582e+11	0	0.99999999999
6	1.99998423e-07	1.577	1.17451602e+11	3.18309886	0.99999999997

Table C.2: Table showing the single-qubit gate fidelity for theoretical driving time t_{theo} and driving frequency w_{theo} for different drives M when we only have AC Stark shift included in our model.

M	F
2	0.9999892552087563
3	0.9999999991759733
4	0.9999974277794634
5	0.9999999967024421
6	0.9999989172259042

Table C.3: Table showing the theoretical and optimized driving time t_{drive} and driving frequency w_{drive} for different drives for the model that includes the resonance frequency shift due to heating and their difference with the idealized case, 200 ns and $1.17451582e11$ rad Hz respectively. We also give the rounded fidelity at the calculated optimal driving time and -frequency.

Drives	Optimal t_{drive} [s]	$\lvert t_{drive} - t_{id}\rvert$ [ns]	Optimal w_{drive} [rad Hz]	$\lvert w_{drive} - w_{id}\rvert$ [MHz]	F
2	2.00661138e-07	0.661	1.17463692e+11	1.927	0.99999999945
3	2.00039884e-07	1.123	1.17467336e+11	2.006	0.99999999997
4	2.01136756e-07	1.137	1.17464637e+11	2.078	0.99999999998
5	2.01250412e-07	1.250	1.17464998e+11	2.135	0.999999999996
6	2.01198604e-07	1.199	1.17465368e+11	2.194	0.999999999991